Available online at www.sciencedirect.com

ScienceDirect

Current Opinion in
Colloid & Interface Science

# Progress in integrated photo-rechargeable battery technologies

Manuel Abellán[1,2,a], Isabel Ciria-Ramos[1,2,a], Ignacio Gascón[1,2], Marta Haro[1,2] and Emilio J. Juarez-Perez[1,3]

Integrated photo-rechargeable battery systems represent a significant advancement in sustainable energy storage and conversion by combining photovoltaic energy harvesting with direct energy storage in a compact design. Although initially studied in the 1970s, interest in this field has surged in recent years. Due to the multidisciplinary nature of this topic, researchers from diverse backgrounds approach it with varying methodologies, resulting in highly diverse cell designs and inconsistent performance metrics. These variations complicate the comparison and evaluation of system efficiency and functionality. This review presents a comprehensive overview of the field's development and current state, from early photoelectrochemical approaches to modern integrated designs. Additionally, it addresses the challenge of performance evaluation by compiling current approaches to performance measurement and proposing standardized evaluation parameters under defined conditions. This dual focus on field overview and metrics standardization aims to provide both a thorough understanding of solar electrochemical energy storage technologies and a framework for their consistent evaluation, which is critical for advancing these technologies.

**Addresses**
[1] Instituto de Nanociencia y Materiales de Aragón (INMA), CSIC-Universidad de Zaragoza, Zaragoza, 50009, Spain
[2] Departamento de Química Física, Facultad de Ciencias, Universidad de Zaragoza, Zaragoza, 50009, Spain
[3] Aragonese Foundation for Research and Development (ARAID). Government of Aragon, Zaragoza, 50018, Spain

Corresponding author: Haro, Marta (mharo@unizar.es)
[a] M.A. and I.C-R. have contributed equally to this work and both of them have the status of first authors in this work.

**Current Opinion in Colloid & Interface Science** 2025, **77**:101915

This review comes from a themed issue on **VSI: Energy Conversion and Storage (2024)**

Edited by **Juan Luis Delgado** and **Sule Erten-Ela**

For a complete overview see the Issue and the Editorial

**https://doi.org/10.1016/j.cocis.2025.101915**



## Introduction

Decarbonization of the energy sector is imperative and depends heavily on advancing technological innovations in renewable energy. While renewable sources exhibit significant potential, they are hindered by their intermittent and variable nature. Solar energy, a prominent example, has the theoretical capacity to meet global energy demands but requires efficient capture and storage systems to address the mismatch between production and consumption.

As of 2023, solar photovoltaic (PV) systems accounted for over 288 GW in Europe, 840 GW in Asia, and 156 GW in North America [1]. These systems are simple to install and involve low maintenance costs. However, the temporal disparity between peak solar generation and residential energy demand leads to suboptimal self-consumption rates. Although some high-tech startups and spin-offs are advancing technologies for integrating PV systems and batteries, PV cells and batteries are currently externally integrated with electronics to facilitate the connection. This modular approach of connecting separate PV panels and batteries offers reasonable convenience for most applications, particularly where specific climate conditions or customized solutions require flexible configurations. However, having a single integrated device that can both generate electricity and store excess energy would be ideal for plug-and-play applications where system optimization and simplified installation are priorities.

Since the 1970s, researchers have explored various strategies to harness solar energy for electrochemical applications. Two main scientific communities have contributed to this field, each with distinct approaches. One is the photoelectrochemical community, focused on utilizing solar energy to drive redox reactions within photoelectrochemical cells (PEC). These reactions include the degradation of pollutants through photooxidation processes, the solar-driven water splitting to produce hydrogen ($H_2$), or the reduction of $CO_2$ into valuable energy vectors. In these systems, solar energy ($h\nu$) is directly converted into chemical energy, stored in

the form of chemical bonds (e.g., moles of $H_2$ or other energy carriers). Additionally, some PEC-based studies have explored energy storage through a third electrode (although there are examples of two and four electrodes), enabling charge accumulation via double-layer capacitance or faradaic processes (measured in F or mA·h, respectively). On the other hand, the photovoltaic research community has focused on converting solar energy into electrical energy by optimizing power output, defined as the product of photovoltage and photocurrent ($V_{ph}$·$I_{ph}$). This electrical power is then measured to determine its efficiency in charging a battery.

In any case, the final goal is to store chemical energy in the battery, which then serves as the power source for generating electrical energy ($\Delta G_0 = -zF\varepsilon^\circ$) to be used on demand. To obtain this chemical energy from the solar energy, light harvesting is critical in the semiconductor materials (e.g. c-Si, halogen perovskite, etc.), and the engineering of selective layers to enhance the efficiency and stability of PV cells and also with catalysts for the final application in the PEC cell.

A key distinction arises when addressing the challenge of charging ion-based batteries, such as Li-ion, Li–S, Li–$O_2$, Na-ion, and Zn-ion systems, as well as redox flow batteries (RFB) and other batteries based on Faradaic processes (such as NiMH batteries). In photoelectrochemistry, it is well established that for a semiconductor to drive a redox reaction, its conduction band (CB) or lowest unoccupied molecular orbital (LUMO) must be aligned with the electrochemical redox potential of the reduction reaction, while its valence band (VB) or highest occupied molecular orbital (HOMO) must be positioned below the redox potential to enable oxidation [2]. Similarly, in Li-, Na-, or Zn-based batteries, where the operating potential is determined by the difference in the chemical potential of the cation between the anode ($\mu_A$) and the cathode ($\mu_C$), precise band alignment is crucial for efficient charge transfer.

Figure 1 provides a comprehensive overview of the energy levels—CB (LUMO) and VB (HOMO)—of key semiconductors used in Solar Electrochemical Energy Storage (SEES) systems, alongside their relative position on the electrochemical scale for cation-ion-based storage systems. This figure highlights that Zn-based battery redox processes can be more effectively driven by semiconductors commonly used in PEC and PV cells. Moreover, redox flow batteries offer the advantage of selecting redox pairs that can be tailored to align the energy bands of the chosen semiconductors. In contrast, PV cells are expected to generate a floating potential, which may reduce/eliminate the necessity for strict band alignment in certain configurations. Likewise, in capacitors and supercapacitors, energy storage occurs

**Figure 1**

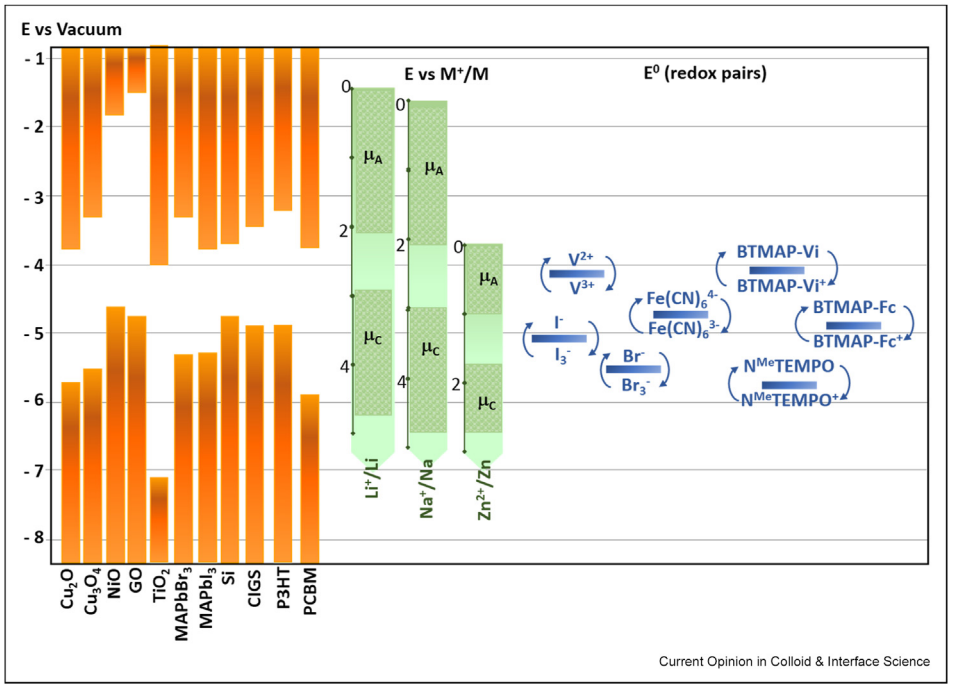


Diagram of CB (LUMO) and VB (HOMO) energies of some of the main semiconductors used in PVs and photoelectrochemistry in relation to the energy scales used in Li-ion, Na-ion, and Zn-ion batteries. The graph also presents the electrochemical redox potentials of commonly used redox pairs in redox flow batteries, referenced against the energy scale relative to vacuum.

electrostatically rather than through Faradaic processes, circumventing this constraint altogether.

This mini-review is organized as follows: Overview provides an overview of the historical evolution of SEES systems. Metrics for evaluating system performance addresses the critical challenge of performance evaluation by analyzing current metrics, their applications, and limitations. Revision metrics reported in the literature presents the metrics reported in the literature. Finally, Challenges and outlook discusses the challenges associated with these metrics and proposes a standardization framework to facilitate easier comparison. It is important to highlight that, while the metrics used in capacitors and redox flow batteries are discussed in this mini-review, the systems analyzed in greater detail are those based on cation chemistry batteries, such as $Li^+$. Excellent review articles are available for solar rechargeable RFB [3–5], and solar rechargeable capacitors [6,7].

## Overview

During the 1970s, significant progress was made in photoelectrochemistry, particularly with the development of the photoelectrochemical cell (PEC) for solar fuel generation, inspired by the work of Fujishima and Honda on $TiO_2$ for water splitting in 1972 [8]. In 1976, Hodes et al. [9,10] introduced the pioneering concept of solar electrochemical energy storage using a PEC, employing CdSe as the photoelectrode, $S/S^{2-}$ as the redox electrolyte, and $Ag_2S/Ag$ as an anode. Concurrently, research also focused on the decomposition of contaminants using photocatalysts, such as the degradation of cyanides proposed by Frank and Bard in 1977 [11].

In the following two decades, the 1980s and 1990s, photoelectrochemical research focused mainly on $H_2$ generation for solar water splitting and photooxidation of contaminants, while SEES research went under the radar. In this period, most of the SEES systems were based on the conversion of solar energy into chemical energy by inducing a redox process, well involving the electrode and electrolyte [12–14] (like Hodes experiments), or a redox process only in the electrolyte [15–18].

Two important advances occurred in 1991: dye-sensitized solar cells (DSSCs) [19] and Li-Ion Batteries (LIBs) [20]. Although both technologies were studied for a long time, this year is considered the year of the birth of DSSCs and the beginning of the commercialization of LIBs. DSSCs can be seen as photoelectrochemical cells, where no overall change in the redox electrolyte composition occurs, using the photocharges for direct generation of electricity. These two advances marked a turning point in the development of SEES systems. DSSCs demonstrated that efficient photoelectrochemical devices could be manufactured through simple solution-processing methods, offering an alternative to traditional semiconductors that require high-purity materials and complex fabrication processes. Meanwhile, the commercialization of LIBs established reliable energy storage architectures with high energy density. The convergence of these two technologies laid the groundwork for integrating molecular photoactive materials with ion intercalation mechanisms, opening new pathways for single-device solar energy conversion and storage [21,22].

In 1995, the first study of SEES based on $Li^+$ intercalation process was conducted [23], utilizing $CuFeTe_2$ layered semiconductor as both a light harvester and active intercalation $Li^+$ material during the charge process. Although this type of system was minimally explored during the 2000s [24,25], it has garnered significant attention since 2018 [26–33], extending to other cations such as $Zn^{2+}$ [34–42] and $Mg^{2+}$ [43]. Another approach, introduced in 2017, involves employing a light harvester distinct from the host material for cation intercalation [44–47]. Beyond Li-ion battery, other mechanisms based on $Li–I_2$ [48], $Li–O_2$ [49–51], and Li–S [52] batteries have also been photo-assisted.

During the 2010s, SEES systems capable of $H_2$ generation have also been investigated. In these systems, the energy stored in the photoanode during light exposure facilitates prolonged $H_2$ production in the cathode during darkness, acting as light harvesters [53–55].

The first adaptation of a photovoltaic cell into a SEES system based on DSSC was in the early 2000s. In these systems, the photocurrent generated in DSSCs induced the (de)intercalation of ions in a charge-storage electrode [56,57] or the accumulation of electrostatic charges forming photo-rechargeable (super)capacitors [58,59]. Throughout the subsequent decade, both of these system types underwent continued investigation, resulting in significant advancements. Studies focused on the intercalation of different ions, including $Li^+$ [22,60–64], $ClO_4^-$ [65], and $Na^+$ [66], and extended to other mechanisms such as $Li–O_2$ [67], flow redox batteries [68–73], and pseudocapacitors [74,75]. Notable work includes the development of photo-rechargeable supercapacitor wires [76–79] for wearable systems.

In the last decade, the studies of PV cells integrated in SEES have been increasing. These systems are mainly photo-rechargeable (super)capacitors and flow redox batteries based on Si [18,80–83], CIGS (copper indium gallium selenide) [84], and bulk heterojunction (BHJ) [85] organic photoactive materials. Additionally, a Li-ion storage mechanism has been reported for BHJ materials [86]. Building on recent advancements in perovskite (PVK)-based photovoltaics, photo-rechargeable systems based on $Li^+$ batteries (Li-ion and Li–S) have been

more recently studied, as well as tandem configurations with Si for photo-rechargeable supercapacitors and flow redox batteries.

A scheme of some representative systems that reflect the evolution of SEES cells based on energy storage in $Li^+$ is represented in Figure 2. The system [61] modified a DSSC by replacing the counter electrode (Pt) with a $WO_3$ charge-storage electrode, capable of $Li^+$ intercalation. Its main limitation is the maximum voltage, determined by the redox potential difference between $WO_3$ lithiation and the DSSC shuttle redox couple ($3I^-/I_3^-$). The work [22] proposed $TiO_2$ nanotubes on Ti sheets for direct electron transfer to a LIB with a $LiCoO_2$ cathode, requiring three DSSC tandems to meet LIB voltage. Later studies explored coupling DSSCs with Li-oxygen [67] and $LiFePO_4$ [63] batteries, showing reduced charging voltages and eventually bypassing the $3I^-/I_3^-$ shuttle. More recently, it has been studied the fusion of PV cell with LIB [86].

## Metrics for evaluating system performance

The development of integrated photo-rechargeable energy systems has led to the emergence of various device architectures, each with its unique set of performance characteristics. To effectively evaluate and compare these systems, it is crucial to establish standardized metrics that capture both the energy conversion and storage aspects of these devices. This section outlines the key performance metrics used in general in the field and divides the metrics by solar-to-electrical energy conversion, solar-to-electrochemical energy conversion, electrochemical-to-electrical conversion, and combined solar-electrochemical-electrical energy conversion metrics.

### Solar-to-electrical energy conversion metrics

a) Photocurrent Density ($j_{ph}$, $mA \cdot cm^{-2}$): This metric quantifies the current generated per unit area of the photo-electrode under illumination. It is a crucial indicator of the ability of the electrodes to convert light into electrical current. For instance, a photocurrent in the range of 600−700 $\mu A\ cm^{-2}$ is estimated for a photo-rechargeable electrode based on $Li_xTiO_2$ nanoparticles [26]. This photocurrent corresponds to a photocharging rate lying between C/2 and C/3, which are very practical charging rates for most applications.

In first studies, the photo-charge quantity ($Q_{ph}$) was defined as the difference between discharge current after the $V_{oc}$ has been reached under light irradiation and in dark conditions. $Q_{ph}$ should not be confused with $j_{ph}$ in which the discharge current is under light illumination.

**Figure 2**

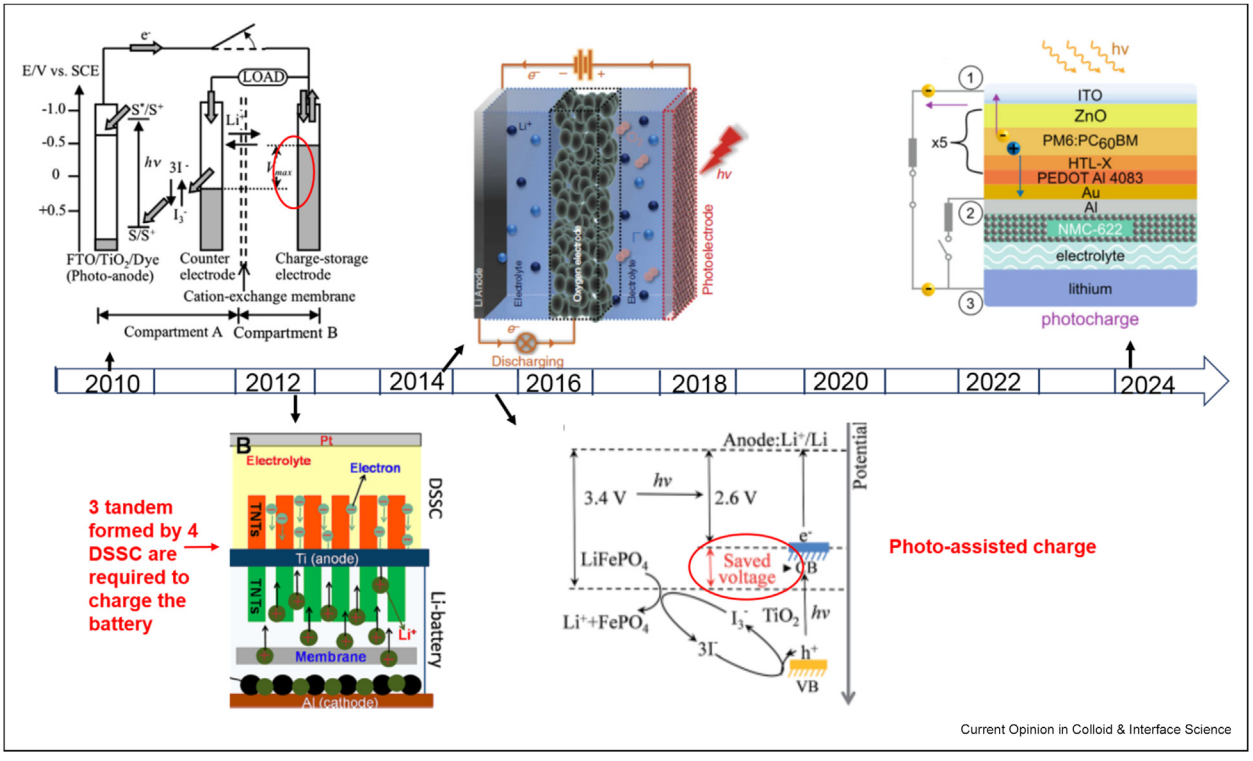


Schemes of the systems proposed in the literature for LIB photocharging at the year of publication. The schemes are taken from references: up row from left to right: [61,67], and [86], down row from left to right: [22], and [63].

b) Quantum Efficiency (*EQE and IQE*): Quantum efficiency, often referred to as Incident Photon-to-Current Efficiency (*IPCE*) in photoelectrochemical systems, measures the ratio of the number of charge carriers collected to the number of photons incident on the device at a given wavelength. It can be expressed as external quantum efficiency (*EQE*) or internal quantum efficiency (*IQE*).

The *EQE* can be calculated using the following equation:

$$EQE(\lambda) = \left(\frac{h \cdot c}{e \cdot \lambda}\right) \cdot \left(\frac{j_{ph}}{P_{in}}\right) \quad (1)$$

where $h$ is Planck constant, $c$ is the speed of light, $e$ is the elementary charge, $\lambda$ is the wavelength of incident light, and $P_{in}$ is the incident solar power density.

For example, reference [87] uses a related concept to calculate the theoretical photocurrent density ($j_{cal}$), equivalent to the previous $j_{ph}$, based on the *EQE*:

$$j_{cal} = e \cdot \int N_{\lambda}(\lambda) \cdot EQE(\lambda) d\lambda \quad (2)$$

where $N_{\lambda}$ is the photon flux spectrum.

*IQE* accounts only for the absorbed photons for the material, and it is calculated:

$$IQE = \frac{EQE}{1 - R(\%)} \quad (3)$$

where R(%) is the reflectance. *IQE* is higher than *EQE* and it only estimates the efficiency of the material to convert the absorbed photons in photocurrent.

c) Power Conversion Efficiency (*PCE*, %): Percentage of incident solar energy converted into electrical energy. It can be expressed mathematically as:

$$PCE\ (\%) = \frac{Electrical\ power\ output}{Incident\ solar\ power} \cdot 100 \quad (4)$$

More specifically, it is the ratio between the maximum electrical power point ($P_{max}$) and the input light power (*Pin*):

$$PCE\ (\%) = \frac{V_{OC} \cdot j_{SC} \cdot FF}{P_{in}} \cdot 100 \quad (5)$$

where $V_{oc}$ is the open-circuit voltage, $j_{sc}$ is the short-circuit current density, *FF* is the fill factor (a measure of the quality of the solar cell) and $P_{in}$ is the input power (from the Sun is standardized at 1000 W/m$^2$ under AM1.5G conditions).

## Solar-to-electrochemical energy conversion metrics

a) Open-circuit Voltage ($V_{OC}$, V): The open-circuit voltage represents the maximum potential difference between the electrodes under illumination with no external load. It is determined by the energy levels of the materials used and the design of the photo-electrode. For example, ~850 mV has been demonstrated in photo-rechargeable zinc-ion capacitors [35]. A similar value, ~850 mV, is reported for a solar flow battery [18].

b) Solar-to-chemical Conversion Efficiency ($\eta_{STC}$, %): This metric represents the efficiency of converting solar energy into stored chemical energy. Different nuances have been defined for this parameter depending on the system [81]. For instance, in a photoelectrochemical cell where solar energy is converted into $H_2$ as an energy carrier, it takes the form:

$$\eta_{H-STC}\ (\%) = \frac{j_{ph} \cdot \left|E_{bias} - E^{0'}\right|}{P_{in}} \cdot 100 \quad (6)$$

where $E_{bias}$ is the applied bias, $E^{0'}$ is the reversible potential of the redox couple (if there is only water 1.23 V), and $P_{in}$ is the incident solar power density.

In the case of a solar redox flow cell, $\eta_{STC}$ can be defined as [81]:

$$\eta_{O-STC}\ (\%) = \frac{j_{op} \cdot \left|E^{0'}_{positive} - E^{0'}_{negative}\right|}{P_{in}} \cdot 100 \quad (7)$$

where $j_{op}$ is the operating photocurrent density, $E^{0'}_{positive}$ and $E^{0'}_{negative}$ are the reversible potentials of the positive and negative redox couples, respectively, and $P_{in}$ is the incident solar power.

c) Light Harvesting Efficiency ($\eta_{LHE}$, %): This metric quantifies the ability of the photo-electrode to absorb incident light. It is calculated using the equation:

$$\eta_{LHE} = \frac{\int \left(I_{S(\lambda)} \cdot A(\lambda) \cdot \left(E_{bandgap} - E_{abs(\lambda)}\right)\right) d\lambda}{\int I_{S(\lambda)} d\lambda} \cdot 100 \quad (8)$$

where $I_{S(\lambda)}$ is the solar spectrum, $A(\lambda)$ is the absorption efficiency, $E_{bandgap}$ is the bandgap energy, and $E_{abs(\lambda)}$ is the energy of absorbed photons. This is not properly a conversion metric, but provides relevant information about the photoactive material.

d) Cycling Stability (capacity retention over cycles): Cycling stability is a crucial metric for assessing the long-term performance of the device. It is typically expressed as the percentage of initial capacity

retained after a certain number of charge−discharge cycles. Discharge plots for photoassisted rechargeable Li−$O_2$ batteries were obtained over 50 cycles [49]. In contrast, supercapacitors are characterized by large cycling stability, particularly when they are compared with batteries where bulk processes are used to damage electrodes along cycling. For example, a ∼90 % capacitance retention over 1000 cycles was demonstrated for photo-rechargeable zinc-ion capacitors [35].

### Electrochemical-to-electrical energy conversion metrics

a) Specific Capacity ($mA \cdot h \cdot g^{-1}$): This metric represents the amount of charge stored per unit mass of the active material. It is a fundamental measure of the energy storage capability of the electrode. Our recent development for solar energy storage using a $Cu_2O$−$TiO_2$ photocathode reported specific capacities of ∼146 mAh $g^{-1}$ for their photo-rechargeable lithium-ion battery [45].
b) Specific Capacitance ($F \cdot g^{-1}$): This metric represents the charge storage capability per unit mass of the active material for capacitor systems. A photo-rechargeable specific capacitance of ∼11,377 mF $g^{-1}$ was reported for zinc-ion capacitors [35].
c) Energy Density ($W \cdot h \cdot kg^{-1}$ or $W \cdot h \cdot L^{-1}$): Energy density quantifies the amount of energy stored per unit mass (gravimetric) or volume (volumetric) of the device. It is crucial for assessing the practical applicability of the system. An energy storage density of 1.15 Wh $L^{-1}$ was reported for an integrated photoelectrochemical solar energy conversion and electrochemical storage device [18].
d) Charge/Discharge Rate (C-rate): The C-rate indicates how fast the battery can be charged or discharged relative to its maximum capacity. Higher C-rates are desirable for rapid energy storage and release.
e) Coulombic Efficiency (*CE*, %): This metric represents the ratio of charge extracted during discharge to the charge input during charging:

$$CE\ (\%) = \frac{(I \cdot t)_{discharge}}{(I \cdot t)_{charge}} \cdot 100 = \frac{Q_{discharge}}{Q_{charge}} \cdot 100 \qquad (9)$$

It indicates the reversibility of the electrochemical processes.

f) Battery Energy Efficiency ($\eta_B$, %): This parameter includes the Voltaic efficiency in the Coulombic Efficiency. This metric measures the electrical energy recovered from the charged battery:

$$\eta_B\ (\%) = \frac{\int (V \cdot I \cdot dt)_{discharge}}{\int (V \cdot I \cdot dt)_{charge}} \cdot 100 \qquad (10)$$

A Coulombic efficiency of ∼95.4 % was reported for photoassisted lithium-iodine redox cells [48].

g) Self-discharge Rate: The self-discharge rate is particularly important for photo-supercapacitors, as it determines how long the harvested energy can be stored without significant loss.

### Combined performance metrics

a) Overall Solar-to-Output Electricity Efficiency ($\eta$, %): *SOEE* or $\eta$ is a comprehensive metric that captures the overall efficiency of converting solar energy to useable electrical energy, including both conversion and storage processes. It is calculated using the equation [18]:

$$SOEE\ (\eta, \%) = \frac{E_{discharging}}{E_{illumination}} \cdot 100 = \frac{\int I_{out} \cdot V_{out} dt}{\int S \cdot A \cdot dt} \cdot 100 \qquad (11)$$

where $E_{discharging}$ is the useable electrical energy delivered, $E_{illumination}$ is the total solar energy input, $I_{out}$ is the output current, $V_{out}$ is the output voltage, $S$ is the solar irradiance, and $A$ is the illuminated area.

b) Photo-charging Rate (C-rate under illumination): This metric indicates how quickly the device can be charged under illumination. It is particularly important for assessing the practical applicability of photo-rechargeable systems. Reference [26] reported photo-charging rates of C/2 to C/3 under standard illumination conditions.
c) Capacity Enhancement under Illumination (*CEI*, %): This metric quantifies the increase in storage capacity when the device is exposed to light compared to dark conditions. Capacity enhancements of 82 % under

$$CEI\ (\%) = \frac{Specific\ Capacity\ (illumination) - Specific\ Capacity\ \ (darkness)}{Specific\ Capacity\ \ (darkness)} \cdot 100 \qquad (12)$$

illumination for a photo-rechargeable Li-ion batteries [35] were calculated as:

where the Specific Capacity is provided in $mA \cdot h \cdot g^{-1}$.

However, in Ref. [29] this parameter appears to be calculated using the specific capacity under illumination in the denominator. The authors report an enhancement in energy efficiency of ~70 %, though they do not specify the equation used to estimate this metric. However, based on the reported specific capacities – 69 mAh $g^{-1}$ in darkness and 162 mAh $g^{-1}$ under illumination—and equation (11), the CEI value is estimated to be ~135 %. Thus, using the specific capacity in darkness as the denominator provides a more accurate representation of the capacity enhancement, aligning more closely with equation (11).

*CEI* parameter is dependent on the current rate. The increase of the rate from 200 mAh g-1 to 2000 mAh g-1 produces the increase of *CEI* value from 17.8 % to 22.8 % in a Li-ion type photobattery [ref. 23-Nanoscale-Boruah]. This effect is probably due to the increase of photoconductivity of the photoelectrode under illumination, as reduced impedance shows. A similar effect is reported for photocapacitors [43].

d) Energy Saving Efficiency (*ESE*, %): Energy saving efficiency represents the reduction in input electrical energy required for charging due to the contribution of solar energy. Reference [88] reported energy savings of ~90 % for their photoassisted chargeable sodium-ion batteries. This estimation is estimated as:

$$ESE\ (\%) = \frac{V_{charging}\ in\ dark - V_{charging}\ under\ illumination}{V_{charging}\ in\ dark} \cdot 100 \tag{13}$$

Sometimes it can be found in the literature as divided by $V_{charging}$ under illumination, such as [63], which provides a value of 20 % and calculated according to equation (13) should be 24 %.

In literature, it can be found another parameter, very similar in name: Efficient Energy Saving (*EES*, %) [27], which compares the better performance of the photobattery under illumination respect in darkness. It can be estimated as:

$$EES\ (\%) = \left( \frac{V_{discharging}\ under\ illumination}{V_{charging}\ under\ illumination} - \frac{V_{discharging}\ in\ dark}{V_{charging}\ in\ dark} \right) \cdot 100 \tag{14}$$

The *EES* value reported in Ref. [27] is 38.7 %, but it would be 16.8 % calculated as *ESE* according to equation (13).

e) Energy Efficiency Increase (*EEI*, %): This parameter is used in photo-assisted batteries, and provides the increase of energy efficiency of the battery when it is illuminated with respect to the same battery working in dark [48]. This parameter can be estimated as:

$$EEI\ (\%) = \frac{\eta_{B,light} - \eta_{B,dark}}{\eta_{B,dark}} \cdot 100 \tag{15}$$

where $\eta_{B,light}$ and $\eta_{B,dark}$ are calculated according to equation (10).

f) Input Power Decrease (*IPD*, %) and Output Power Increase (*OPI*, %): In these parameters both energy and capacity are considered, and they measure the contribution of the solar energy in decreasing the required power of charge and increasing the output power of the photobattery [31]. These parameters can be calculated as:

$$IPD\ (\%) = \frac{\left( \int_0^t V_{charge} \cdot I_{charge} \cdot dt \right)_{light}}{\left( \int_0^t V_{charge} \cdot I_{charge} \cdot dt \right)_{dark}} \tag{16}$$

$$OPI\ (\%) = \frac{\left( \int_0^t V_{discharge} \cdot I_{discharge} \cdot t_{discharge} dt \right)_{light}}{\left( \int_0^t V_{discharge} \cdot I_{discharge} \cdot t_{discharge} dt \right)_{dark}} \tag{17}$$

*IPD* considers also the reduction of time in charging with respect *ESE*, and OPI includes the voltage output respect *CEI*.

g) Round-trip Efficiency (*RTE*, %): Round-trip efficiency represents the overall efficiency of the charge—discharge cycle, including both solar charging and electrical discharging [51]:

$$RTE\ (\%) = \frac{V_{discharging}\ under\ illumination}{V_{charging}\ under\ illumination} \cdot 100 \tag{18}$$

h) Capacity Utilization Rate (%): This metric indicates in flow-batteries how effectively the system utilizes the available capacity of the electrolyte. Reference [89] demonstrated a capacity utilization rate higher than 80 % for their long-lifetime aqueous organic solar flow battery.

In conclusion, the evaluation of integrated photo-rechargeable energy systems requires a comprehensive set of metrics that capture both the energy conversion and storage aspects of these devices. By standardizing these metrics across different system types, researchers can more effectively compare and optimize the performance of various photo-rechargeable technologies. Figure 3 summarizes the metrics found in the literature. As the field continues to evolve, it is likely that new metrics will emerge to address the unique characteristics of novel device architectures and materials.

## Revision metrics reported in the literature

### Systems based on storing energy photoelectrode

This section addresses SEES systems that design a photoelectrode based on a single material (such as Cu-HHB [32]) or composite (such as $Cu_2O$ as light harvester and $TiO_2$ as a storing element [45]), serving the dual role of solar light harvesting and energy storing. Table 1 presents examples of such systems with their reported metrics. Although a direct comparison is not feasible due to experimental measurement conditions, the table provides an overview of the most commonly used metrics and their respective value ranges.

The first column specifies the light energy used, although in some cases this information is unavailable. The second column describes the system using nomenclature similar to that of galvanic cells in IUPAC conventions. In this notation, the anode material of the SEES system appears on the left, followed by the electrolyte, and the cathode on the right. The light-harvesting element(s) are highlighted in black. Components in different phases are separated by "|", whereas those forming part of the same element, such as COF or NF that constitute the photoelectrode in Ref. [27] are separated by a comma. Below, the configuration (either 2/3 electrodes or an adapted coin cell) is also specified. The subsequent columns present the metrics defined in Metrics for evaluating system performance, along with the corresponding references. Explicitly reported values are provided, while those calculated or estimated from the data in the original work or extracted from graphs are underlined.

In SEES systems based on the $Li^+$ electrochemical energy storage mechanism, pioneering studies adapted the photoelectrode as an anode capable to intercalate Li ions. This is the case for the previously mentioned $CuFeTe_2$ compound, which was immersed in a nonaqueous cell connected via a salt bridge to an aqueous cell containing an Ag/AgCl reference electrode, where a voltage decrease of ~130 mV was observed in the presence of light [23]. A similar behavior was observed for $TiO_2$ photoelectrodes obtained by laser deposition techniques [24,25], which use Pt as the reference electrode. In these studies, the reported metrics were the voltage change under illumination ($V_{ph}$) and the photocharge ($Q_{ph}$), defined as the difference in extracted charge when the cell is discharged in the dark after being in open-circuit conditions under both light illumination and darkness.

In the past decade, research on photoelectrodes has shifted toward their use as battery cathodes. For instance, light induces the delithiation of a $TiO_2$ photocathode in a three-electrode cell (with two Li foil electrodes), achieving an internal power conversion efficiency of 0.5 % [26]. Various semiconductor combinations with hole-blocking and electron-transport layers have been employed to enhance photocharge separation. Examples include $MoS_2/MoO_x$ system with a SOEE ($\eta$) of 0.05 % [29], and a $V_2O_5$/P3HT/rGO photoelectrode with a $\eta \sim 0.22$ % [30], both tested

**Figure 3**

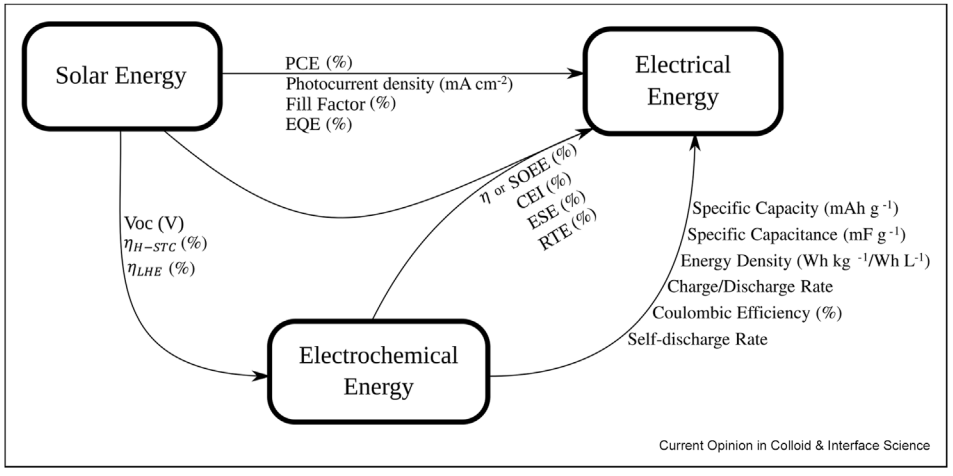


Main metrics utilized to evaluate the conversion of solar-to-electrical energy, solar-to-electrochemical energy, electrochemical-to-electrical and solar-to-electrochemical-to-electrical energy indicated inside the triangle.

under solar simulators. Operando optical microscopy studies on $V_2O_5$/P3HT/rGO revealed that $Li^+$ migrates from within $V_2O_5$ to its surface, with some ions subsequently released into the electrolyte [90]. The two materials strategy smooths the photocharge separation, reducing the need for $e^-$ or $h^+$ selective layers. Additionally, the light-harvesting material remains electronically stable during (de)lithiation processes. For example, $LiFePO_4$ was paired with N719 Ru dye as photoactive material (η of 0.06%—0.08 %) [44], and perylene diimide dye (PDI) [46]. In the latter case, PDI was blended with PEO to obtain a photoactive binder, though with minimal response to light. Finally, in a $Cu_2O/TiO_2$ system, photoinduced holes efficiently transfer from $Cu_2O$ to $TiO_2$, promoting delithiation and achieving $\eta = 0.29$ %. However, photoelectron injection for lithiation is hindered by the position of $TiO_2$ CB [45]. This limitation is analyzed in a proposed energetic landscape, offering insights for future photoelectrode design.

Most SEES systems focusing on the delithiation process of the cathode operate in a half-cell configuration, using Li metal foil as a counter electrode. Since Li metal has one of the highest redox potentials, it is unlikely that photoelectrons can spontaneously reduce $Li^+$ at the anode, as inferred from Figure 1. Therefore, metrics assessing the enhancement of LIB (dis)charge capacities (*CEI*) or energy output (*OPI*), evaluating the reduction in energy input (*ESE* and *IPD*), the improvement of the battery working under illumination or in darkness (*EES*, *EEI*), and the overall energy efficiency *(RTE*) are particularly relevant.

For instance, in the bidimensional Covalent Organic Framework (COF) formed by 4,5,8-naphthalenediimide (NDI) and triphenylamine (TPA), light induces the formation of the $TPA^+$-$NDI^-$ complex, which reacts with $Li^+$ and galvanostatically injected electrons, forming TPA-$NDI^-$-$Li^+$. As a result, the specific capacity exceeded the theoretical value, yielding an EES value of 38.7 % [27]. Light also enhances the battery energy output under illumination, as observed for $C_{60}$ guest inside of a porous organic cage [31], with an *OPI* of 81.4 % and *IPD* of 13.2 %. In the $TiO_2/LiFePO_4$ system, where $TiO_2$ acts as the light harvester and LiFePO4 as $Li^+$ -host [47], illumination increases capacity (*CEI* = 4.6 %), but no significant differences in charge/discharge voltages were observed (estimated *ESE* ∼0 % from the graphs).

Other SEES systems are based on Li—$O_2$, Li—$I_2$, and Li—S batteries. In Li—$O_2$, photo-assisted charging helps overcome the large overpotentials associated with the charging process. When illuminated, the bimetallic Fe-UiO-66 MOF shows a decrease in charging voltage to 3.56 V [51], yielding an RTE value of 96 %. However, the best results are obtained with g-$C_3N_4$, with or without a redox mediator ($I^-/I_3^-$), where the oxidation of $Li_2O_2$ occurs at 1.9 V (*RTE* = 142 %) [49], and 1.96 V (*RTE* = 140 %) [50], respectively. Similarly, α-$Fe_2O_3$ photoelectrode induces the oxidation of $I^-$ anions to $I_3^-$ lowering the charge voltage from ∼4.13 V to ∼3.43 V in Li—$I_2$ battery (*ESE* = 27.2 % and estimated *EEI* = 20 %) [48]. Other systems based on CdS—$TiO_2$ [52], and $Bi/Bi_2O_3/TiO_2$ [91] have also been reported for Li—S photobatteries, where photoholes oxidize the $Li_2S$ species present in the electrolyte. For these systems, *SOEE* values as high as 2.3 % [52] and 2.58 % [91] have been reported.

The high energy required for photoelectrons to reduce or intercalate $Li^+$ at the anode can be significantly lowered by using alternative cations, such as $Mg^{2+}$ and $Zn^{2+}$, or by charging a capacitor, which relies on a voltage difference rather than specific CB or VB levels of the light harvesters (Figure 1). Additionally, these systems enable the use of nonflammable aqueous electrolytes, a key advantage given that prolonged solar exposure may increase SEES temperatures.

Some examples of $Zn^{2+}$ photobatteries, where Zn foil is the anode and the photoelectrode plays a dual role of solar energy harvesting and $Zn^{2+}$ intercalation, include $V_2O_5$/P3HT/rGO (which can be scaled to build a photo-pouch cell) [34], ZnO/$MoS_2$ [37], $V_2O_5$/rGO [38], $V_2O_5$/Ag nanowires [36], and ZnO/$VO_2$ [39]. Among these, the highest *SOEE* (η) is reported for ZnO/$MoS_2$, which is ∼1.8 % under ∼455 nm light and ∼0.2 % with a solar simulator. The record *SOEE* value of 3.9 % was achieved using a $TiO_2$/CuTPP/Cu:$V_2O_5$ photoelectrode, and Zn flakes with activated carbon as the anode [42]. This system is capable of transferring photoelectrons from the CB of a photoactive material to the higher-energy CB of another via Förster Resonance Energy Transfer to enhance charge generation.

With the addition of a porous carbon as hole transportation layer, a high photovoltage of 0.8 V is obtained for ZnO/CdS/porous carbon photocapacitor [40]. A $Mg^{2+}$-based photocapacitor with rGO/$V_2O_5$ and activated carbon counter electrode increases the galvanostatic capacity up to 56 % under illumination (at ∼455 nm) [43].

### Systems containing all the elements of a PV cell

This section discusses SEES systems based on various PV technologies: dye-sensitized, organic (bulk heterojunction), silicon, and perovskite solar cells. Dye-sensitized solar cells (DSSCs), which involve direct charge transfer between the light harvester and the liquid electrolyte, could also be included in the previous section. Table 2 presents examples of these SEES systems, categorized by PV technology. The second column, labeled “system”, follows the same

**Table 1**

**Metrics reported and estimated on SEES systems based on a photoelectrode (single material or hybrid) with the dual function of light harvesting and electrochemical energy storage. The table is divided by the mechanism of energy storage. The system is described: from left to right – negative electrode; followed by the electrolyte – positive electrode. The light-harvesting element is marked in black. Italic values are estimated from data/graphs collected in the paper, but are not explicitly stated in the text.**

| Light Source | System | $V_{oc}$ (V) | Capacity/ Capacitance/Energy under illumination | SOEE (η, %) | CEI (%) (OPI, %) | ESE (%) (IPD, %) | RTE (%) (EES, %) (EEI, %) | Ref. |
|---|---|---|---|---|---|---|---|---|
| Li-ion | | | | | | | | |
| Xe lamp (50 W) | **$CuFeTe_2$**\|$LiClO_4(CH_3CN)$\|Pt<br>2 Electrodes | | 0.56 Wh $kg^{-1}$ | | | | | [23] |
| 3 W $cm^{-2}$ | **FTO \|CFs,$TiO_2$, $Li_xTiO_2$**\|$LiCl_4$ (0.5 M, $CH_3CN$)\|CF<br>3 Electrodes (Ref: Pt) | 0.15 V | *230 μC $cm^{-2}$* | | | | | [24] |
| 3 W $cm^{-2}$ | **FTO \|$TiO_2$, $Li_xTiO_2$**\|$LiCl_4$ (0.5 M, $CH_3CN$)\|CF<br>3 Electrodes (Ref: Pt) | 0.15 V | *40* μC $cm^{-2}$ | | | | | [25] |
| Solar Simulator | Li\|$LiPF_6$ (1 M, EC:DMC)\|**$LiFePO_4$,$FePO_4$, Ru dye N19**\|FTO<br>3 Electrodes (Ref: Li foil) | | | 0.06 %–0.08 % | | | | [44] |
| 100 $mWcm^{-2}$ | Li\|$LiPF_6$ (EC:DEC:VC)*\|**$TiO_2$, $Li_xTiO_2$**\|FTO<br>3 Electrodes (Ref: Li foil)<br>*alternative: LiTFSI (EMI.TFSI) | 3 V | | 0.5 % | | | | [26] |
| 100 $mWcm^{-2}$ | Li\|$LiPF_6$ (1 M, EC:DMC:DEC)\|**COF,** NF\|Ni (f)<br>2 Electrodes: adapted CR2025 | | | | | | 117 %<br>(EES = 38.7 %) | [27] |
| 100 $mWcm^{-2}$ | Li\|LiPF6(1 M-electrolyte)\|<br>**(C6H9C2H4NH3)2PbX4,PCBM**\|FTO<br>2 electrodes | | *~0.6* m*Wh* | 0.034 % | | | | [92] |
| 100 $mWcm^{-2}$ | Li\|$LiPF_6$ (1.2 M, EC:EMC)\|**$LiMn_2O_4$, $Mn_2O_4$**\|Al (m)<br>2 Electrodes | | | | *43*<br>*(OPI = 181)* | | | [28] |
| 100 $mWcm^{-2}$ | Li\|$LiPF_6$ (1 M, EC:EMC\|**$MoS_2$, $MoO_2$**\|ITO<br>2 Electrodes | | | 0.05 % | *24 %* | | | [29] |
| 100 $mWcm^{-2}$ | Li\|LiTFSI (EC:PC)\|**$V_2O_5$, P3HT, rGO**\|CF<br>2 Electrodes: adapted CR2032 | | | 0.22 %<br>(2.6 % at 455 nm) | 57 % | | | [30] |
| 200 $mWcm^{-2}$ | Li\|LiTFSI (1 M, DOL:DME)\|**C60@POC**\|FTO<br>2 Electrodes | | | 1 % | (81.4 %) | *24 %*<br>*(13.2 %)* | (*EEI* = 81.4 %) | [31] |
| 100 $mWcm^{-2}$ | Li\|$LiPF_6$(1 M, EC:DEC)\|$TiO_2$,**$Cu_2O$**\|ITO<br>CR2032 | | | 0.29 % | | | | [45] |
| 100 $mWcm^{-2}$ | Li\|LiTFSI (5 M, EC:PC)\|**Cu-HHB**\|Al (m)<br>2 Electrodes | | | | 17.8–22.8 % | | | [32] |
| ~12 mW $cm^{-2}$; ~455 nm | Li\|LiTFSI (5 M, EC:PC)\|**H–$V_2O_5$**\|Al (s)<br>2 Electrodes: adapted CR2032 | | | | 24.4 % | 5.7 %<br>(9.7 %) | | [33] |
| 100 $mWcm^{-2}$ | $FePO_4$\|LiTFSI (aq)\| $LiFePO_4$,**p(pD1-EO)**<br>3 electrode (Swagelok, ref. Ag/AgCl(3 M)) | | | | 11 % | | | [46] |
| Not found | Li\|$LiPF_6$ (EC:DMC)\|LiFePO4,**$TiO_2$**<br>2 Electrodes | | | | 4.6 % | 0 % | | [47] |
| 125 $mWcm^{-2}$<br>365 nm | Li\|LiTFSI (1 M, DOL:DME)\|**Co(bpy) (dhbq)$_2$**<br>2 Electrodes: adapted CR2025 | | | 0.33 % | | | | [93] |
| Li–$I_2$ | | | | | | | | |
| 100 $mWcm^{-2}$ | Cu\|Li\|LiTFSI (EC:DMC)⁞LiI + KI + $I_2$(aq)\|α-$Fe_2O_3$\|FTO<br>⁞ LATP<br>2 Electrodes | | 180 mAh $g^{-1}$ | | | 27.2 | (*EEI* = 20 %) | [48] |

| | | | | | | | |
|---|---|---|---|---|---|---|---|
| Li–$O_2$ | | | | | | | |
| Xe-lamp | Li\|LitFSI(G4)\|$LiO_2$,$O_2$,**$C_3N_4$**,CP<br>2 Electrodes | 375 mAh $g^{-1}$ | | | | 140 % | [50] |
| Xe-lamp | Li\|LiTFSI(1 M, TEGDME)\|$LiO_2$,$O_2$,**FeUiO-66**,CP<br>2 Electrodes: adapted CR2032 | | | | 12.3 | 96 %<br>(EES = *27.3* %) | [51] |
| Li–S | | | | | | | |
| 50 mW $cm^{-2}$ | Li\|Electrolyte\|$L_2S$,$S_8$,CC,**CdS**,**$TiO_2$** | | 2.3 % | *26* % | 4.0 | 96.8 %<br>(EES = 7.2 %) | [52] |
| 60 mW $cm^{-2}$ | Li\|LiTFSI, DOL:DME,$LiNO_3$\|$L_2S$,$S_8$,CC,**$Bi$**,**$Bi_2O_3$**,**$TiO_2$**<br>2 Electrodes: adapted CR2032 | | 2.58 % | *25* % | | | [91] |
| 50 mW $cm^{-2}$ | Li\|Li-electrolyte\|**S@Khaust-1**,**QDs(CsPbBr$_3$/Cs$_4$PbBr$_6$)**\|CF<br>2 Electrodes: adapted CR2032 | | 0.24 % | | | | [94] |
| Zn-ion | | | | | | | |
| 2–12 mW $cm^{-2}$; 455 nm | Zn\|Zn$(CF_3SO_3)_2$(aq)\|**$VO_2$**,**P3HT**,**rGO**,**CF**<br>2 Electrodes: adapted CR2450 | | 1.2 % | *94.7* % | *32.8* % | | [34] |
| 100 mW$cm^{-2}$ | Ni(f)\|Zn-FIs-AC\|$ZnCl_2$(γ-BL)\|$Zn_xCu$:$V_2O_5$,**CuTPP**,**$TiO_2$**\|FTO<br>2 Electrodes | 2.4 V | 3.9 % | | | | [42] |
| 100 mW$cm^{-2}$ | Zn\|Zn$(OTf)_2$(aq)\|**$V_2O_5$**\|ITO<br>2 Electrodes: adapted CR2032 | | | 54 % | | | [41] |
| Capacitor | | | | | | | |
| ~50 mW $cm^{-2}$; ~420 nm | Zn\|$ZnSO_4$(aq)\|**g-$C_3N_4$**\|FTO<br>2 Electrodes | 0.85 V | 0.01 % | 82 % | | | [35] |
| 12 mW $cm^{-2}$; 455 nm | AC\|Mg$(NO_3)_2$(aq)\|**$VO_2$**,**rGO**,**CF**<br>2 Electrodes | | | 82 % | | 24.2%–56.0 % | [43] |

nomenclature as Table 1, though most of these systems use 3 electrodes, one of which is shared between the PV and the battery/capacitor components. In this case the common electrode is underlined. Among the different metrics reported in Metrics for evaluating system performance, the most commonly reported for these systems are $V_{oc}$, capacity/capacitance/energy under illumination, and *SOEE*. In contrast, the parameters related to input energy saving and/or output energy enhancement are scarcely reported, and the parameters that compare the battery under illumination and in darkness have not been found, and excluded in Table 2. Here the systems with 4-electrodes are not reviewed.

Pioneering works using DSSCs for SEES employed 2-electrode systems, with a $TiO_2$ layer on top of $WO_3$ layer, soaked with a lithium $I^-/I_3^-$ electrolyte and a transparent platinized-FTO glass as the secondary electrode [56]. Under illumination, the generated photoelectron in $TiO_2$/dye transfers to the $WO_3$, forcing $Li^+$ intercalation, while the photohole oxidizes the redox $I^-/I_3^-$ redox couple regenerating the dye. In discharging, $Li^+$ deintercalates and $I_3^-$ is reduced to $I^-$ in the Pt cathode. The system achieved a maximum open circuit voltage of 0.6 V (which is the potential difference between the redox active pair and the lithiation potential of $WO_3$), and stored 1.8C $cm^2$ at 1 Sun, with a *SOEE* of 0.55 %. However, the performance of 2 electrodes remains suboptimal due to the intricate interactions between the photoelectrode, energy storage reactions, and the electrolyte. For example, rapid capacity fading was observed in $WO_3$/CdS system due to degradation from photogenerated holes and exposure to $I_3^-$ [64]. As a result, most PV-SEES are based on 3- or 4-electrode architectures.

DSSC-based SEES systems built with 3-electrode designs allow the use of two distinct and optimized electrolytes for each unit: photocharging and charge-storage units, separated by an ion-permeable membrane. For example, Selemion™ $Li^+$-exchange membrane is used in Ref. [57], with a *SOEE* value of 0.5−1%, and an increasing charge storage of 8.5 mC $cm^{-2}$. An increase of *SOEE* up to 3.2 % and 38 mC/$cm^{-2}$ [60] is obtained by depositing the Pt counter electrode and Ppy storage-electrode on top of a patterned FTO substrate. A cation-selective membrane was electrophoretically deposited on top of the PPy electrode allowing the use of a single electrolyte. The use of $WO_3$ in the SEES increases the capacity of approximately 37.8 mC/$cm^2$, the *SOEE* to 3.21 %, and the cycling retention with respect to Ppy [61].

Highly-ordered $TiO_2$ nanotube arrays can replace the expensive Pt electrocatalyst. A TiN electrode, fabricated by nitridation of $TiO_2$ nanotubes, increased electroactive sites, enhancing the discharge capacity

(CEI = 40 %) [62]. $TiO_2$ nanotubes can also be grown on both sides of a titanium sheet [22], acting as both the photoelectrode and anode, paired with $LiCoO_2$ as the cathode. Three solar cells in series achieved a $V_{OC}$ of 3 V, a *SOEE* of 0.82 %, and a storage capacity of ~0.04 mAh; though no area or mass data were provided.

These systems can also intercalate other cations, such as $Na^+$. $Fe_2(MoO_4)_3$ microspheres [66] sotred $Na^+$ as $Na_xFe_2(MoO_4)_3$, achieving a capacity of 0.04 mAh $cm^{-2}$. The redox pair $I^-/I_3^-$ has also been applied as a mediator to reduce the charging voltage in Li–$O_2$ battery [67], lowering the overpotential by ~0.7 V. Additionally, a $LiFePO_4$ cathode in a semicell configuration demonstrated an *ESE* = 24 % [63].

One of the advantages of 3-electrode configuration is the possibility to connect several PV cells to reach the desirable voltage for battery charging. For example, the organic solar cells (OSC) on PM6:$PC_{60}BM$ donor:-acceptor pair provided a voltage of 0.94 V. A series of five such cells was used to achieve the necessary voltage to charge a Li battery, employing $LiNi_{0.6}Mn_{0.2}Co_{0.2}O_2$ (NMC622) as the cathode in a semicell configuration (Figure 2) [86], though no metrics are provided.

Si PV cells have been used in SEES coupled with NiH–$Ni(OH)_2$ batteries, achieving the highest reported *SOEE* values: 14.5 % [95] and 18.2 % [96]. The later system enables continuous load operation, supplying power both from the solar cell under illumination and from the battery in darkness.

In SEES systems using perovskite solar cells, two different configurations have been reported: i) a perovskite solar cell fused with an electrochemical energy storage system and ii) a perovskite material serving as both a light harvester and Li-ion battery cathode. While the latter configuration could be better integrated in Table 1, presenting both approaches here facilitates their direct comparison.

In systems where the perovskite material functions solely as a light harvester, the reported *SOEE* values are significantly higher than when it also serves as the cathode. In Ref. [97], a dense carbon layer acts as a hole-selective layer for the perovskite solar cell, interfacing with a more porous carbon loaded with sulfur, which serves as the cathode of Li–S battery. This system achieves a SOEE value of 5.9 % and a capacity of 750 mAh $g^{-1}$. In a multilayered configuration consisting of n-type ZnTe, $C_{60}$, CdS, perovskite ($CH_3NH_3PbI_3$), and InAlGaP/InGaP fused with capacitor composed of two carbon nanotubes (CNTs) electrodes separated by a dielectric, a *SOEE* of 11.81 % is achieved. However, when the perovskite material also functions as $Li^+$ host cathode, the reported *SOEE* values are considerably lower, at 0.034 % [92] and 0.05 % [98].

### SEES systems based on redox flow batteries (RFB)

RFBs are characterized by the use of two redox pairs in the electrolyte, which can be strategically selected to align the energy bands of the light absorber(s)—the CB with the anolyte and the VB with the catholyte—as illustrated in Figure 1. The key performance metrics for these systems typically include $V_{oc}$, capacity, and *SOEE*, while other parameters, such as *RTE*, are less frequently reported. These metrics are compiled in Table 3 for few SEES examples based on RFBs. More comprehensive reviews on these systems are available in Refs. [3,4].

To accommodate the low-voltage conditions of PV materials (commonly <0.7 V), recent research has explored inorganic/organic electrolytes, allowing finer tuning of the cell voltage compared to conventional inorganic redox couples. In terms of redox pair selection, early studies predominantly employed the $I_3^-/I^-$ couple [68–70], whereas more recent efforts have shifted toward organic redox pairs, such as BTMAP-Vi/BTMAP-Fc [83,100].

Notably, RFB-based SEES systems generally achieve high SOEE values, with the current record of 20.1 % using a Si-perovskite tandem [101].

## Challenges and outlook

The integration of photovoltaic energy harvesting with electrochemical storage represents a promising pathway for sustainable energy systems, particularly in portable electronics and remote applications. The parameter that better reflects this integration is **Overall Solar-to-Output Electricity Efficiency** (*SOEE*, $\eta$). However, while this technology is still in its early stages, systems based on electrostatic double-layer storage, such as supercapacitors, or redox flow batteries generally achieve better performance metrics than those relying on electrochemical storage, such as Li-ion batteries. This is primarily because supercapacitors do not involve redox processes; eliminating the need for charge transfer with a species undergoing a redox reaction and making them independent of the energy level alignment of the light harvester. Additionally, the flexibility to select different redox pairs in flow batteries significantly enhances *SOEE*, with the highest reported value reaching 20.3 %.

Typically, supercapacitors offer high power but low energy density, making them more suitable for applications such as wearables or sensors. Conversely, RFBs are generally designed for large-scale energy storage, limiting their portability. Therefore, the development of portable, photo-rechargeable electronics based on Li-ion or similar batteries remains in an earlier stage of technological progress.

**Table 2**

**Metrics reported and estimated on SEES systems based on a complete PV cell (DSSC, organic, etc) connected to an electrochemical energy storage through a common electrode 3 or 4 electrodes configuration. In a 3-electrode configuration, the underline electrode is common between the photovoltaic and electrochemical energy storage systems. The system is described: from left to right – negative electrode; followed by the electrolyte – positive electrode. The light-harvesting element is marked in black. Italic values are estimated from data/graphs collected in the paper, but are not explicitly stated in the text.**

| Light Source | System | $V_{oc}$ (V) | Capacity/ Capacitance/ Energy under illumination | SOEE (η, %) | CEI (%) (OPI, %) | ESE (%) | RTE (%) | Ref |
|---|---|---|---|---|---|---|---|---|
| DSSC | | | | | | | | |
| 100 mWcm$^{-2}$ | FTO\|**$WO_3$, $TiO_2$, dye**\|LiI(PC)\|Pt<br>2 Electrodes | 0.6 | 1.8C cm$^{-2}$ | 0.6 % | | | | [56] |
| 100 mWcm$^{-2}$ | FTO\|**$TiO_2$,Ru-dye\|LiI($CH_3CN$)\|Pt**,AC $(CH_3CH_2)_4NBF_4$\|AC<br>2 electrodes | 0.45 V | 0.69 F cm$^{-2}$ | | | | | [58] |
| 100 mWcm$^{-2}$ | FTO\|**$TiO_2$,N3Dye**\|LiI,$I_2$(PC)\|*Pt*\| LiI,$I_2$(PC)⁞ $LiClO_4$(PC)\|PPy | 0.6 V | | 22*% | | | | [57] |
| 100 mWcm$^{-2}$ | FTO\|**$TiO_2$,Ru-dye**\|C8H15IN2,LiI,I2 **($CH_3CN$)\|*Pt***\|AC $(CH_3CH_2)_4NBF_4$\|AC<br>3 electrodes | 0.8 V | 47 μWh cm$^{-2}$ | | | | | [59] |
| 100 mWcm$^{-2}$ | FTO\|**$TiO_2$,N719Dye**\|LiI,$I_2$($CH_3CN$)\|*Pt*\| LiI,$I_2$($CH_3CN$)\|PPy\|FTO<br>3 electrodes | | 37.8 mC cm$^{-2}$ | 3.21 % | | | | [60] |
| 100 mWcm$^{-2}$ | FTO\|**$TiO_2$,Dye**\|LiI,$I_2$(MPN)\|*Pt*\| LiI,$I_2$(MPN)⁞ Li-electrolyte\|$WO_{3-x}$\|FTO<br>3 electrodes | | 4.57C | | | | | [61] |
| 100 mWcm$^{-2}$ | Graphene,Cu(m)\|LiI,$I_2$ (TBP,MPN)\|**N719-Dye, ZnO NWs**\|*Au covering plastic μ-fiber*\| ZnO NWs \|$H_3PO_4$,PVA(w)\|Graphene, Cu(m)<br>3 electrodes | 0.1 V | ~0.4 F cm$^{-2}$ | | | | | [76] |
| 100 mWcm$^{-2}$ | CNTs\| LiI,$I_2$($CH_3CN$)\| **N719Dye, $TiO_2$**\|Ti(w)\|CNTs\|$H_3PO_4$,PVA(w)\|CNTs | 0.6 V | | 1.5 % | | | | [77] |
| 100 mWcm$^{-2}$ | FTO\|PPy,PPy-$ClO_4^-$\|$LiCl_4$(PC)\|***Pt*\|PEDOT,**<br>**PEDOT $^+$ $ClO_4^-$\|Dye\|$TiO_2$**\|FTO<br>3 electrodes | 0.76 | 8 mAh g$^{-2}$ | ~0.1 % | | | | [65] |
| 100 mWcm$^{-2}$ | FTO\|**$TiO_2$,N719Dye**\|LiI,$I_2$(MPN)\|Ti(mesh)/TiN\| LiI,$I_2$(MPN)⁞$WO_3$,CNT<br>3 electrodes | 0.7 V | 0.15 mAh cm$^{-2}$ | | 40 %<br>OPI = 69.5 | | | [62] |
| 100 mWcm$^{-2}$ | Pt\| LiI,$I_2$,TBP(MPN)\| **$TiO_2$**(NTs)**,N749Dye**\|*Ti*\|$TiO_2$ (NTs)\| $LiPF_6$ (EC,DMC)\|$LiCoO_2$\|Al<br>Tandem DSSC<br>3 electrodes | 3 V | 38.89 μAh | 0.82 % | | | | [22] |
| Xe-lamp | Li\|$LiClO_4$ (EC,DMC)\|$LiFePO_4$, Ti (m)\|$Li_2SO_4$, LiI (w)\| **$TiO_2$**\|Ti(m)<br>3 electrodes | | 100 mAh g$^{-2}$ | | | 24 % | 121 % | [63] |
| 100 mWcm$^{-2}$ | FTO\|**$TiO_2$, Z907Dye**\|$I^-$,$I_2$(org)\|*Ti(mesh)/Pt*\|Na-electrolyte \|$Fe_2(MoO_4)_3$\| FTO<br>3 electrodes | 0.63 V | 0.04 mAh cm$^{-2}$ | | | | | [66] |
| 100 mWcm$^{-2}$ | FTO\|**$WO_3$, $TiO_2$, CdS**\|LiI + $I_2$,(PC)\|Pt<br>2 Electrodes | | 7.3 μAh cm$^{-2}$ | | | | | [64] |
| Organic Solar Cell | | | | | | | | |
| 100 mWcm$^{-2}$ | *Li*\|$LiPF_6$(EC:DMC)\|NMC\|Al\|Au\|PEDOT Al 4083\|HTL-X\|**PM6:$PC_{60}$BM**\|ZnO\|ITO<br>3 electrodes | | *0.45* m*Ah* | | | | | [86] |
| Silicon | | | | | | | | |
| 135.3 mWcm$^{-2}$ | **Au–Zn,Au\|$Al_xGa_yAs$\|GaAs\|Si**\|*Au–Sb,Au*\|$Ni_{x-1}H$\|KOH(aq)\|Ni(OH)2<br>3 electrodes | 1.2–1.3 | | 18.2 % | | | | [96] |
| | SS(m)\|AC\|KOH(aq)\|NHC\|**Ni(f)\|Ti(f)\|Ag(p)\|Si(w)\|<br>Cu(f)** | 1.19 V | 125 W Kg$^{-1}$ | 14.5 % | | | | [95] |

(*continued on next page*)

**Table 2. (*continued*)**

| Light Source | System | $V_{oc}$ (V) | Capacity/ Capacitance/ Energy under illumination | SOEE (η, %) | CEI (%) (OPI, %) | ESE (%) | RTE (%) | Ref |
|---|---|---|---|---|---|---|---|---|
| | 2 Si cells in serie<br>3 electrodes | | | | | | | |
| Perovskite<br>100 mWcm$^{-2}$ | ITO\|CNT\|**InAlGaP, InGaP\|$CH_3NH_3PbI_3$\|C60**\|CNT\|<br>$HfO_2$(dielectric)\|CNT<br>3 electrodes | *1.4 V* | | 11.81 % | | | | [99] |
| 100 mWcm$^{-2}$ | Li \| LiTFSI (1 M, DOL) \|C@ $S_8$,$Li_2S$\| **C\| $CH_3NH_3PbI_3$ \|$TiO_2$\|** FTO<br>3 electrodes | | 750 mAh g$^{-1}$ | 5.9 % | | | | [97] |
| Solar Simulator | FTO\|**c-$TiO_2$, mp-$TiO_2$/$MA_3Bi_2I_9$**\|Pt\|FTO<br>2 electrodes | | | 0.05 % | | | | [98] |

For advancing SEES based on batteries, two main strategies can be considered: (i) developing a photoelectrode and approaching SEES system as a PEC cell, where photogenerated charge carriers directly drive the desired redox process, or (ii) using a PV cell to drive an energy storage system via a common electrode. The first approach requires precise energy alignment, significantly limiting the range of photo-rechargeable systems, whereas, in the PV-based approach, multiple cells can be connected to achieve the required $V_{oc}$ for battery charging. As a result, PV-based SEES typically achieve higher *SOEE* values than those relying on photoelectrodes. However, a key challenge in PV-driven SEES is the need for three-electrode devices, whereas PEC-based configurations are often studied in two-electrode setups adapted from coin cells.

A potential advantage of photoelectrodes is their ability to assist in charging batteries that require a high energy input. For example, in Li—$O_2$ batteries, where charging occurs at a significantly higher voltage than discharge, photo-assisted charging could provide a substantial benefit. To evaluate the efficacy of photassistance, various efficiency metrics have been introduced.

- **Energy discharge enhancement**: *CEI*, which considers only the mAh increase, and *OPI*, which also accounts for the voltage at which discharge occurs. While *CEI* is more commonly reported, *OPI* is more relevant for technological applications.
- **Charge energy reduction due to light exposure**: *ESE*, which accounts only on charging voltage reduction, and *IPD*, which additionally considers current and charging time. Since comparisons are typically made under the same applied current, *IPD* directly measures the reduction in charging time due to light.
- **Battery performance improvement under illumination**: Metrics such as *EES* and *EEI* compare the battery's operation in light versus darkness. However, in the literature, the term "energy savings" is often used without explicitly defining the equation used, leading to potential confusion due to the lack of standardization.
- **Overall energy efficiency**: *RTE*, the most commonly reported metric, measures the ratio of energy extracted from the battery to the energy required for charging under illumination. Notably, *RTE* values exceeding 100 % have been reported, indicating that the extracted energy surpasses the input energy needed for charging.

To simplify the interpretation of SEES studies, which often employ diverse experimental configurations, we propose the following recommendations:

**Standardized cell labeling:** We suggest adopting a labeling system for photo-rechargeable cells based on

**Table 3**

**Metrics reported and estimated on SEES systems based on redox flow batteries: Solar Redox Flow Batteries (SRFB). The system is described in two parts the photoelectrodes and the redox pair. The light-harvesting element is marked in black. Italic values are estimated from data/graphs collected in the paper, but are not explicitly stated in the text.**

| Light Source | Photoelectrodes | Redox Pairs | $V_{oc}$ (V) | Capacity under illumination | SOEE (η %) | RTE (%) | Ref |
|---|---|---|---|---|---|---|---|
| 40 mW $cm^{-2}$ | FTO\|$TiO_2$,dye\|LISICON\|Pt\|FTO | $DMFc^+/DMFcI_3^-/I^-$ | 0.6 | 70 μAh | *0.04 %* | | [68] |
| 100 mW $cm^{-2}$ | FTO\|$TiO_2$,N719dye\|LiI(TBP)\|Pt\|Ti(m) | $Li_{2+x}WO_4/Li_2WO_4I_3^-/I^-$ | 0.7 | 20 mAh $L^{-1}$ | | | [69] |
| 100 mW $cm^{-2}$ | FTO\|$TiO_2$,N719dye\|LiI(TBP)\|Pt\|Ti(m) | $(C_8H_6N_2)^{x-}I_3^-/I^-$ | 0.8 | 30 mAh $L^{-1}$ | 1.2 % | | [70] |
| | p-Si\|n-Si | $AQDS/AQDSH_2Br_3^-/Br^-$ | | 471 mAh $L^{-1}$ | 3.4 % | | [81] |
| 100 mW $cm^{-2}$ | $TiO_2$\|Si | $Fe(CN)_6^{4-}/Fe(CN)_6^{3-}$TEMPO-Sulfate | 1.6 | | | | [102] |
| 300 mW $cm^{-2}$ | Si multijunction cell | $VO^+_2/VO^{2+}V^{3+}/V^{2+}$ | 1.7 | 24 mA $cm^{-2}$ | 12.3 % | 6 | [82] |
| | $p^+$Si\|n$^+$Si\|n$^+$Si\|Ti\|$TiO_2$\|Pt | BTMAP-Vi/ BTMAP-Fc | 0.35 | | 5.4 % | | [83] |
| | $(FAPbI_3)_{0.83}(MAPbBr_3)_{0.17}$\|Si Tandem cell | BTMAP-Vi/ $N^{Me}$-TEMPO | 1.36 | | 20.1 % | | [101] |
| 100 mW $cm^{-2}$ | SJ GaAs cell | BTMAP-Vi/ BTMAP-Fc | | | 13.3 % | | [100] |

galvanic cell notation, where the light-harvesting component is highlighted in **bold**, the common electrode in a three-electrode configuration is **underlined**, and semipermeable membranes are marked with ⁞. Additionally, we have observed that in some studies, the electrolyte composition is not explicitly specified, which should be avoided for clarity.

- **Standardized labeling**: We suggest an adapted IUPAC galvanic cell notation, where the light harvester is highlighted in bold, the common electrode in three-electrode configurations is underlined, and semipermeable membranes are represented with a specific notation, ⁞. In addition, electrolyte composition should always be explicitly stated.
- **Consistent *SOEE* reporting**: To facilitate comparison, *SOEE* ($\eta$) should be reported under the standard illumination condition of 100 mW $cm^{-2}$, specifying the light source, while also allowing additional measurements at other power intensities if needed.
- **Equation transparency**: While we have compiled the most frequently reported metrics, other parameters are also used. Until the metrics is not well established, the equation used for their calculation should be clearly stated or referenced.
- **Current standardization**: Since performance improvements depend on charging/discharging currents, specifying the applied current is essential. Standardizing measurements at fixed rates, such as 0.1C and 1C, would enhance data comparability.

The distinction between research backgrounds is evident in the literature, with differences in approach depending on whether the study originates from PV or battery expertise. Establishing a common set of metrics for this emerging field will be crucial for fostering collaboration and accelerating technological development.

While this work has focused primarily on efficiency metrics, stability—both in terms of charge retention and cycle life—is another critical factor for SEES viability. These systems must overcome both the degradation mechanisms of solar cells and the cycling limitations of batteries, making long-term stability a key challenge. Additionally, the optimal operating conditions for solar cells and batteries often differ, adding another layer of complexity to device integration. However, despite these challenges, the potential benefits of SEES—particularly in terms of cost reduction, sustainability, and energy decentralization—are significant. By integrating energy generation and storage within a single system, SEES could reduce grid dependency and enhance energy accessibility in remote locations. Addressing these technological hurdles will be essential for unlocking the full potential of SEES, paving the way for scalable and efficient solar-powered storage solutions.

## Declaration of competing interest

The authors declare that they have no known competing financial interests or personal relationships that could have appeared to influence the work reported in this paper.

## Acknowledgements

The authors acknowlege the project PID2022-140516OB-I00 funded by MICIU/AEI 10.13039/501100011033 and FEDER, EU. M. H. also acknowledges the project CNS2023-145197 funded by MICIU/AEI /10.13039/501100011033 and the European Union NextGenerationEU/PRT

## Data availability

No data was used for the research described in the article.

## References

Papers of particular interest, published within the period of review, have been highlighted as:

* of special interest
** of outstanding interest


1. Sucharitakul S, Goble NJ, Kumar UR, Sankar R, Bogorad ZA, Chou FC, Chen YT, Gao XPA: **Intrinsic electron mobility exceeding 103 cm2/(V s) in multilayer InSe FETs**. *Nano Lett* 2015, **15**:3815–3819.
2. Guerrero A, Haro M, Bellani S, Antognazza MR, Meda L, Gimenez S, Bisquert J: **Organic photoelectrochemical cells with quantitative photocarrier conversion**. *Energy Environ Sci* 2014, **7**:3666–3673.
3. Lu P, Leung P, Su H, Yang W, Xu Q: **Materials, performance, and system design for integrated solar flow batteries–A mini review**. *Appl Energy* 2021, **282**, 116210.
4. Wedege K, Bae D, Smith WA, Mendes A, Bentien A: **Solar redox flow batteries with organic redox couples in aqueous electrolytes: a minireview**. *J Phys Chem C* 2018, **122**: 25729–25740.
5. Bae D, Kanellos G, Faasse GM, Dražević E, Venugopal A, Smith WA: **Design principles for efficient photoelectrodes in solar rechargeable redox flow cell applications**. *Communications Materials* 2020, **1**:17.
6. Nithya VD: **Recent research in the development of integrated solar cell supercapacitors**. *J Electron Mater* 2025:1–20.
7. Kumar BA, Ran F, Maram PS, Sangaraju S: **Progressive horizons of energy generation and storage: nook and cranny of photo-supercapacitors**. *J Energy Storage* 2024, **97**, 112876.
8. Fujishima A, Honda K: **Electrochemical photolysis of water at a semiconductor electrode**. *Nature* 1972, **238**:37–38.
9. Hodes G, Manassen J, Cahen D: **Photoelectrochemical energy conversion and storage using polycrystalline chalcogenide electrodes**. *Nature* 1976, **261**:403–404.
10. Manassen J, Hodes G, Cahen DF. In *Photo-electrochemical cell containing chalcogenide redox couple and having storage capability*. Google Patents; 1977.
11. Frank SN, Bard AJ: **Heterogeneous photocatalytic oxidation of cyanide and sulfite in aqueous solutions at semiconductor powders**. *J Phys Chem* 1977, **81**:1484–1488.
12. Yonezawa Y, Okai M, Ishino M, Hada H: **A photochemical storage battery with an n-GaP photoelectrode**. *Bull Chem Soc Jpn* 1983, **56**:2873–2876.
13. Kanbara T, Takada K, Yamamura Y, Kondo S: **Photo-rechargeable solid state battery**. *Solid State Ionics* 1990, **40**:955–958.
14. Hada H, Takaoka K, Saikawa M, Yonezawa Y: **Energy conversion and storage in solid-state photogalvanic cells**. *Bull Chem Soc Jpn* 1981, **54**:1640–1644.
15. Ang PG, Sammells AF: **Photoelectrochemical systems with energy storage**. *Faraday Discuss Chem Soc* 1980, **70**:207–222.
16. Licht S, Hodes G, Tenne R, Manassen J: **A light-variation insensitive high efficiency solar cell**. *Nature* 1987, **326**:863.
17. Fujinami T, Mehta MA, Shibatani M, Kitagawa H: **Polymer electrolyte bilayer films with photorechargeable battery characteristics**. *Solid State Ionics* 1996, **92**:165–169.
18. Li W, Fu HC, Li L, Cabán-Acevedo M, He JH, Jin S: **Integrated photoelectrochemical solar energy conversion and organic redox flow battery devices**. *Angew Chem Int Ed* 2016, **55**: 13104–13108.
19. O'regan B, Grätzel M: **A low-cost, high-efficiency solar cell based on dye-sensitized colloidal TiO2 films**. *Nature* 1991, **353**:737–740.
20. Goodenough JB, Whittingham MS, Yoshino A: *The nobel prize in chemistry 2019, for the development of lithium-ion batteries*. 2019.
21. Gregg BA: **Photoelectrochromic cells and their applications**. *Endeavour* 1997, **21**:52–55.
22. Guo W, Xue X, Wang S, Lin C, Wang ZL: **An integrated power pack of dye-sensitized solar cell and Li battery based on double-sided TiO2 nanotube arrays**. *Nano Lett* 2012, **12**: 2520–2523.
23. Nomiyama T, Kuriyaki H, Hirakawa K: **Photo-rechargeable battery using new layer compound CuFeTe2**. *Synth Met* 1995, **71**:2237–2238.
24. Zou X, Maesako N, Nomiyama T, Horie Y, Miyazaki T: **Photo-rechargeable battery with TiO2/carbon fiber electrodes prepared by laser deposition**. *Sol Energy Mater Sol Cell* 2000, **62**: 133–142.
25. Usui H, Miyamoto O, Nomiyama T, Horie Y, Miyazaki T: **Photo-rechargeability of TiO2 film electrodes prepared by pulsed laser deposition**. *Sol Energy Mater Sol Cell* 2005, **86**:123–134.
26. Andriamiadamanana C, Sagaidak I, Bouteau G, Davoisne C, Laberty-Robert C, Sauvage F: **Light-induced charge separation in mixed electronic/ionic semiconductor driving lithium-ion transfer for photo-rechargeable electrode**. *Adv Sustain Sys* 2018, **2**, 1700166.
27. Lv J, Tan YX, Xie J, Yang R, Yu M, Sun S, Li MD, Yuan D, Wang Y: **Direct solar-to-electrochemical energy storage in a functionalized covalent organic framework**. *Angew Chem* 2018, **130**:12898–12902.
28. Lee A, Vörös M, Dose WM, Niklas J, Poluektov O, Schaller RD, Iddir H, Maroni VA, Lee E, Ingram B: **Photo-accelerated fast charging of lithium-ion batteries**. *Nat Commun* 2019, **10**:1–7.
29. Kumar A, Thakur P, Sharma R, Puthirath AB, Ajayan PM, Narayanan TN: **Photo rechargeable Li-ion batteries using nanorod heterostructure electrodes**. *Small* 2021, **17**, 2105029.
30. Boruah BD, Wen B, De Volder M: **Light rechargeable lithium-ion batteries using V2O5 cathodes**. *Nano Lett* 2021, **21**: 3527–3532.
31. ** Zhang X, Su K, Mohamed AGA, Liu C, Sun Q, Yuan D, Wang Y, Xue W, Wang Y: **Photo-assisted charge/discharge Li-organic battery with a charge-separated and redox-active C 60@ porous organic cage cathode**. *Energy Environ Sci* 2022, **15**: 780–785.
This study demonstrates the dual functionality of $C_{60}$@POC as both a charge separator and a redox-active material. The resulting cathode for photo-assisted Li-organic batteries achieved efficient charge separation and prolonged carrier lifetimes, enhancing solar-to-electrochemical energy storage.
32. Andersen H, Lu Y, Borowiec J, Parkin IP, De Volder M, Boruah BD: **Photo-enhanced lithium-ion batteries using metal–organic frameworks**. *Nanoscale* 2023, **15**:4000–4005.
33. Lu Y, Andersen H, Wu R, Ganose AM, Wen B, Pujari A, Wang T, Borowiec J, Parkin IP, De Volder M, Boruah BD: **Hydrogenated V2O5 with improved optical and electrochemical activities for photo-accelerated lithium-ion batteries**. *Small* 2024, **20**, 2308869.
34. Boruah BD, Mathieson A, Wen B, Feldmann S, Dose WM, De Volder M: **Photo-rechargeable zinc-ion batteries**. *Energy Environ Sci* 2020, **13**:2414–2421.
35. Boruah BD, Mathieson A, Wen B, Jo C, Deschler F, De Volder M: **Photo-rechargeable zinc-ion capacitor using 2D graphitic carbon nitride**. *Nano Lett* 2020, **20**:5967–5974.
36. Boruah BD, Wen B, Nagane S, Zhang X, Stranks SD, Boies A, De Volder M: **Photo-rechargeable zinc-ion capacitors using V2O5-activated carbon electrodes**. *ACS Energy Lett* 2020, **5**: 3132–3139.

37. Boruah BD, Wen B, De Volder M: **Molybdenum disulfide–zinc oxide photocathodes for photo-rechargeable zinc-ion batteries**. *ACS Nano* 2021, **15**:16616–16624.

38. Boruah BD, Mathieson A, Park SK, Zhang X, Wen B, Tan L, Boies A, De Volder M: **Vanadium dioxide cathodes for high-rate photo-rechargeable zinc-ion batteries**. *Adv Energy Mater* 2021, **11**, 2100115.

39. Boruah BD, De Volder M: **Vanadium dioxide–zinc oxide stacked photocathodes for photo-rechargeable zinc-ion batteries**. *J Mater Chem A* 2021, **9**:23199–23205.

40. Liu X, Andersen H, Lu Y, Wen B, Parkin IP, De Volder M, Boruah BD: **Porous carbon coated on cadmium sulfide-decorated zinc oxide nanorod photocathodes for photo-accelerated zinc ion capacitors**. *ACS Appl Mater Interfaces* 2023, **15**:6963–6969.

41. Zha W, Ruan Q, Ma L, Liu M, Lin H, Sun L, Sun Z, Tao L: **Highly stable photo-assisted zinc-ion batteries via regulated photo-induced proton transfer**. *Angew Chem Int Ed* 2024, e202400621.

42. ** Naskar S, Maity D, Dixit A, Freitag M, Kumari K, Singh SK, Deepa M: **A Förster resonance energy transfer enabled photo-rechargeable battery with an energetically misaligned Cu-porphyrin dye/Cu: $V_2O_5$ photocathode**. *J Mater Chem A* 2024, **12**:15203–15226.

This study demonstrates a photo-rechargeable $Zn^{2+}$ ion battery utilizing a FRET-enabled photocathode, achieving significant photo-conversion efficiency and robust cycling stability without external bias.

43. Park SK, Boruah BD, Pujari A, Kim BM, De Volder M: **Photo-enhanced magnesium-ion capacitors using photoactive electrodes**. *Small* 2022, **18**, 2202785.

44. * Paolella A, Faure C, Bertoni G, Marras S, Guerfi A, Darwiche A, Hovington P, Commarieu B, Wang Z, Prato M: **Light-assisted delithiation of lithium iron phosphate nanocrystals towards photo-rechargeable lithium ion batteries**. *Nat Commun* 2017, **8**, 14643.

This study describes the design of a photocathode using lithium iron phosphate (LFP) nanocrystals as a hybrid photo-cathode combined with N719 dye. The system achieves direct photo-oxidation of LFP, facilitating reversible lithium extraction under light exposure. Although the *SOEE* is modest (0.06–0.08%), the study provides useful insights into the processes occurring inside the photo-rechargeable battery.

45. ** Ciria-Ramos I, Juarez-Perez EJ, Haro M: **Solar energy storage using a Cu2O-TiO2 photocathode in a lithium battery**. *Small* 2023, 2301244.

This study presents an energy scheme for charge transfer between the photoactive material ($Cu_2O$) and the $Li^+$-ion storage material ($TiO_2$), highlighting the importance of semiconductor electrochemistry in the design of photoelectrodes for photo-rechargeable batteries.

46. Briqueleur E, Dollé M, Skene W: **A multifunctional binder capable of harvesting light, electronic transport, and photo-charging a lithium-ion photobattery**. *J Mater Chem C* 2024.

47. Cui C, Wang X, Zhu H, Jin Y, Li Y, Pang B, Shang M, Dong H, Yu L, Dong L: **Photo-assisted enhancement of lithium-ion battery performance with a LiFePO4/TiO2 composite cathode**. *Ceram Int* 2024.

48. Nikiforidis G, Tajima K, Byon HR: **High energy efficiency and stability for photoassisted aqueous lithium–iodine redox batteries**. *ACS Energy Lett* 2016, **1**:806–813.

49. Liu Y, Li N, Wu S, Liao K, Zhu K, Yi J, Zhou H: **Reducing the charging voltage of a Li–O 2 battery to 1.9 V by incorporating a photocatalyst**. *Energy Environ Sci* 2015, **8**:2664–2667.

50. Liu Y, Li N, Liao K, Li Q, Ishida M, Zhou H: **Lowering the charge voltage of Li–O 2 batteries via an unmediated photo-electrochemical oxidation approach**. *J Mater Chem A* 2016, **4**:12411–12415.

51. Yang Y, Hu X, Wang G, Han J, Zhang Q, Liu W, Xie Z, Zhou Z: **Two better than one: enhanced photo-assisted Li-O2 batteries with bimetallic Fe-UiO-66 metal-organic framework photocathodes**. *Adv Funct Mater* 2024, 2315354.

52. Liu Y-H, Qu J, Chang W, Yang C-Y, Liu H-J, Zhai X-Z, Kang Y, Guo Y-G, Yu Z-Z: **A photo-assisted reversible lithium-sulfur battery**. *Energy Storage Mater* 2022, **50**:334–343.

53. Xia X, Luo J, Zeng Z, Guan C, Zhang Y, Tu J, Zhang H, Fan HJ: **Integrated photoelectrochemical energy storage: solar hydrogen generation and supercapacitor**. *Sci Rep* 2012, **2**:981.

54. Safshekan S, Herraiz-Cardona I, Cardenas-Morcoso D, Ojani R, Haro M, Gimenez S: **Solar energy storage by a hetero-structured BiVO4–PbO x photocapacitive device**. *ACS Energy Lett* 2017, **2**:469–475.

55. Lemsi A, Cardenas-Morcoso D, Haro M, Gil-Barrachina C, Aranda C, Maghraoui-Meherzi H, García-Tecedor M, Giménez S, Julián-López B: **Lead sulfide nanocubes for solar energy storage**. *Energy Technol* 2020, **8**, 2000301.

56. Hauch A, Georg A, Krašovec UO, Orel B: **Photovoltaically self-charging battery**. *J Electrochem Soc* 2002, **149**:A1208–A1211.

57. Nagai H, Segawa H: **Energy-storable dye-sensitized solar cell with a polypyrrole electrode**. *Chem Commun* 2004:974–975.

58. Miyasaka T, Murakami TN: **The photocapacitor: an efficient self-charging capacitor for direct storage of solar energy**. *Appl Phys Lett* 2004, **85**:3932–3934.

59. Murakami TN, Kawashima N, Miyasaka T: **A high-voltage dye-sensitized photocapacitor of a three-electrode system**. *Chem Commun* 2005:3346–3348.

60. Saito Y, Ogawa A, Uchida S, Kubo T, Segawa H: **Energy-storable dye-sensitized solar cells with interdigitated nafion/poly-pyrrole–Pt comb-like electrodes**. *Chem Lett* 2010, **39**:488–489.

61. Saito Y, Uchida S, Kubo T, Segawa H: **Surface-oxidized tungsten for energy-storable dye-sensitized solar cells**. *Thin Solid Films* 2010, **518**:3033–3036.

62. Yan N, Li G, Pan G, Gao X: **TiN nanotube arrays as electro-catalytic electrode for solar storable rechargeable battery**. *J Electrochem Soc* 2012, **159**:A1770–A1774.

63. Li Q, Li N, Ishida M, Zhou H: **Saving electric energy by integrating a photoelectrode into a Li-ion battery**. *J Mater Chem A* 2015, **3**:20903–20907.

64. Wang Z, Chiu HC, Paolella A, Zaghib K, Demopoulos GP: **Lithium photo-intercalation of CdS-sensitized WO3 anode for energy storage and photoelectrochromic applications**. *ChemSusChem* 2019.

65. Liu P, Yang H, Ai X, Li G, Gao X: **A solar rechargeable battery based on polymeric charge storage electrodes**. *Electrochem Commun* 2012, **16**:69–72.

66. Gui Y-Y, Ai F-X, Qian J-F, Cao Y-L, Li G-R, Gao X-P, Yang H-X: **A solar rechargeable battery based on the sodium ion storage mechanism with Fe 2 (MoO 4) 3 microspheres as anode materials**. *J Mater Chem A* 2018, **6**:10627–10631.

67. Yu M, Ren X, Ma L, Wu Y: **Integrating a redox-coupled dye-sensitized photoelectrode into a lithium–oxygen battery for photoassisted charging**. *Nat Commun* 2014, **5**:5111.

68. Liu P, Cao YI, Li GR, Gao XP, Ai XP, Yang HX: **A solar rechargeable flow battery based on photoregeneration of two soluble redox couples**. *ChemSusChem* 2013, **6**:802–806.

69. Yan N, Li G, Gao X: **Solar rechargeable redox flow battery based on Li 2 WO 4/LiI couples in dual-phase electrolytes**. *J Mater Chem A* 2013, **1**:7012–7015.

70. Yan N, Li G, Gao X: **Electroactive organic compounds as anode-active materials for solar rechargeable redox flow battery in dual-phase electrolytes**. *J Electrochem Soc* 2014, **161**:A736–A741.

71. Yu M, McCulloch WD, Beauchamp DR, Huang Z, Ren X, Wu Y: **Aqueous lithium–iodine solar flow battery for the simultaneous conversion and storage of solar energy**. *J Am Chem Soc* 2015, **137**:8332–8335.

72. McCulloch WD, Yu M, Wu Y: **pH-tuning a solar redox flow battery for integrated energy conversion and storage**. *ACS Energy Lett* 2016, **1**:578–582.

73. Fan L, Jia C, Zhu YG, Wang Q: **Redox targeting of Prussian blue: toward low-cost and high energy density redox flow**

**battery and solar rechargeable battery**. *ACS Energy Lett* 2017, **2**:615–621.

74. Sun H, You X, Deng J, Chen X, Yang Z, Chen P, Fang X, Peng H: **A twisted wire-shaped dual-function energy device for photoelectric conversion and electrochemical storage**. *Angew Chem Int Ed* 2014, **53**:6664–6668.

75. Wang Q, Chen H, McFarland E, Wang L: **Solar rechargeable batteries based on lead–organohalide electrolyte**. *Adv Energy Mater* 2015, **5**, 1501418.

76. Bae J, Park YJ, Lee M, Cha SN, Choi YJ, Lee CS, Kim JM, Wang ZL: **Single-fiber-based hybridization of energy converters and storage units using graphene as electrodes**. *Adv Mater* 2011, **23**:3446–3449.

77. Chen T, Qiu L, Yang Z, Cai Z, Ren J, Li H, Lin H, Sun X, Peng H: **An integrated "energy wire" for both photoelectric conversion and energy storage**. *Angew Chem Int Ed* 2012, **51**:11977–11980.

78. Fu Y, Wu H, Ye S, Cai X, Yu X, Hou S, Kafafy H, Zou D: **Integrated power fiber for energy conversion and storage**. *Energy Environ Sci* 2013, **6**:805–812.

79. Chen X, Sun H, Yang Z, Guan G, Zhang Z, Qiu L, Peng H: **A novel "energy fiber" by coaxially integrating dye-sensitized solar cell and electrochemical capacitor**. *J Mater Chem A* 2014, **2**:1897–1902.

80. Westover AS, Share K, Carter R, Cohn AP, Oakes L, Pint CL: **Direct integration of a supercapacitor into the backside of a silicon photovoltaic device**. *Appl Phys Lett* 2014, **104**, 213905.

81. Liao S, Zong X, Seger B, Pedersen T, Yao T, Ding C, Shi J, Chen J, Li C: **Integrating a dual-silicon photoelectrochemical cell into a redox flow battery for unassisted photocharging**. *Nat Commun* 2016, **7**, 11474.

82. Urbain F, Murcia-López S, Nembhard N, Vázquez-Galván J, Flox C, Smirnov V, Welter K, Andreu T, Finger F, Morante JR: **Solar vanadium redox-flow battery powered by thin-film silicon photovoltaics for efficient photoelectrochemical energy storage**. *J Phys Appl Phys* 2018, **52**, 044001.

83. Li W, Kerr E, Goulet MA, Fu HC, Zhao Y, Yang Y, Veyssal A, He JH, Gordon RG, Aziz MJ: **A long lifetime aqueous organic solar flow battery**. *Adv Energy Mater* 2019.

84. Li W, Fu H-C, Zhao Y, He J-H, Jin S: **14.1% efficient monolithically integrated solar flow battery**. *Chem* 2018, **4**:2644–2657.

85. Zhang Z, Chen X, Chen P, Guan G, Qiu L, Lin H, Yang Z, Bai W, Luo Y, Peng H: **Integrated polymer solar cell and electrochemical supercapacitor in a flexible and stable fiber format**. *Adv Mater* 2014, **26**:466–470.

86. * Büttner J, Delgado R, Wessling R, Wang Y, Esser B, Würfel U, Fischer A: **Energy harvesting and storage with a high voltage organic inorganic photo-battery for Internet of Things applications**. *Energy Technol* 2024, 2301421.
This study introduces a compact, high-voltage photobattery combining a stacked organic solar cell with an NMC 622 battery, specifically designed to power IoT devices efficiently without external voltage boosting.

87. Li T-T, Yang Y-B, Zhao B-S, Wu Y, Wu X-W, Chen P, Gao X-P: **Photo-rechargeable all-solid-state lithium– sulfur batteries based on perovskite indoor photovoltaic modules**. *Chem Eng J* 2023, **455**, 140684.

88. Li Q, Li N, Liu Y, Wang Y, Zhou H: **High-safety and low-cost photoassisted chargeable aqueous sodium-ion batteries with 90% input electric energy savings**. *Adv Energy Mater* 2016, **6**, 1600632.

89. Gelmetti I, Montcada NF, Pérez-Rodríguez A, Barrena E, Ocal C, García-Benito I, Molina-Ontoria A, Martín N, Vidal-Ferran A, Palomares E: **Energy alignment and recombination in perovskite solar cells: weighted influence on the open circuit voltage**. *Energy Environ Sci* 2019, **12**:1309–1316.

90. ** Pandya R, Mathieson A, Boruah BD, de Aguiar HB, de Volder M: **Interrogating the light-induced charging mechanism in Li-ion batteries using operando optical microscopy**. *Nano Lett* 2023, **23**:7288–7296.
Optical microscopy was used to study (de)lithiation in $Li_xV_2O_5$ particles under various conditions, revealing Li-rich phase accumulation and partial delithiation, while demonstrating that, during discharge under light, the photoelectrode is simultaneously charged, increasing the energy extractable by an external device.

91. Yi S, Su Z, Chen H, Zhao Z, Wang X, Zhang Y, Niu B, Long D: **Bi/Bi2O3/TiO2 heterojunction photocathode for high-efficiency visible-light-driven lithium-sulfur batteries: advancing light harvesting and polysulfide conversion**. *Appl Catal, B: Environment and Energy* 2024, **348**, 123853.

92. Ahmad S, George C, Beesley DJ, Baumberg JJ, De Volder M: **Photo-rechargeable organo-halide perovskite batteries**. *Nano Lett* 2018, **18**:1856–1862.

93. Chen L, Ullah Z, Sun H, Yu S, Li W, Chen M, Liu L, Li Q: **Dramatic enhancement in lithium-ion battery capacity through synergistic effects of electronic transitions in light-assisted organic coordination cathode material Co (bpy)(dhbq) 2**. *Energy Storage Mater* 2025, **74**, 103891.

94. Liu Y, Wu F, Hu Z, Zhang F, Wang K, Li L, Chen R: **Regulating sulfur redox kinetics by coupling photocatalysis for high-performance photo-assisted lithium-sulfur batteries**. *Angew Chem* 2024, e202402624.

95. * Song Z, Wu J, Tu Y, Sun L, Zhu T, Li G, Wang X, Du Y, Deng C, Chen Q: **Photocapacitor integrating voltage-adjustable hybrid supercapacitor and silicon solar cell generating a Joule efficiency of 86%**. *Energy Environ Sci* 2022, **15**:4247–4258.
This study presents a three-terminal integrated photocapacitor (IPC) that combines solar energy harvesting and storage, using a voltage-adjustable hybrid supercapacitor (VAHSC) as the storage unit and a silicon solar cell (SSC) as the photovoltaic unit. By optimizing the voltage–current-power coupling between these units, the system achieves an impressive overall efficiency of 15.49%, a Joule efficiency of 86.01%, and excellent charge/discharge cycle stability.

96. Wang B, Licht S, Soga T, Umeno M: **Stable cycling behavior of the light invariant AlGaAs/Si/metal hydride solar cell**. *Sol Energy Mater Sol Cell* 2000, **64**:311–320.

97. * Chen P, Li GR, Li TT, Gao XP: **Solar-driven rechargeable lithium–sulfur battery**. *Adv Sci* 2019, **6**, 1900620.
This study introduces the first integrated perovskite solar cell (PSC)/Li–S solar-driven rechargeable battery using a novel Joint Electrode Mode (JEM). The system achieves a power conversion efficiency (PCE) of 5.14, it also demonstrates a high specific capacity of 750 mAh $g^{-1}$ under ultrafast photocharging (2C).

98. Wang K, Chen Z, Zhang R, Li X, Xu J, Jing H, Zhang P, Liu M, Li S: **Bifunctional MA3Bi2I9 towards solar energy conversion and storage for all-solid-state photo-rechargeable battery**. *J Energy Storage* 2024, **104**, 114561.

99. Farhadi B, Marriam I, Yang S, Zhang H, Tebyetekerwa M, Zhu M, Ramakrishna S, Jose R, Zabihi F: **Highly efficient photovoltaic energy storage hybrid system based on ultrathin carbon electrodes designed for a portable and flexible power source**. *J Power Sources* 2019, **422**:196–207.

100. * Fu H-C, Li W, Yang Y, Lin C-H, Veyssal A, He J-H, Jin S: **An efficient and stable solar flow battery enabled by a single-junction GaAs photoelectrode**. *Nat Commun* 2021, **12**:156.
This study demonstrates the highe SOEE value of 15.4% in a single-junction GaAs solar flow battery (SFB) using a back-illuminated n-p-n photoelectrode. The integration of a $TiO_2$ protection layer and robust aqueous organic redox couples ensures long-term stability (408 h, 150 cycles).

101. ** Li W, Zheng J, Hu B, Fu H-C, Hu M, Veyssal A, Zhao Y, He J-H, Liu TL, Ho-Baillie A: **High-performance solar flow battery powered by a perovskite/silicon tandem solar cell**. *Nat Mater* 2020, **19**:1326–1331.
This study reports a record-high solar-to-output electricity efficiency (SOEE) of 20.1% in integrated solar flow batteries (SFBs) using perovskite/silicon tandem solar cells and BTMAP-Vi/NMe-TEMPO redox couples. The device also demonstrates enhanced capacity utilization, long-term stability, and cost-effective fabrication, making it a strong candidate for off-grid energy applications and advancing practical solar energy storage solutions.

102. Wedege K, Bae D, Dražević E, Mendes A, Vesborg PC, Bentien A: **Unbiased, complete solar charging of a neutral flow battery by a single Si photocathode**. *RSC Adv* 2018, **8**:6331–6340.